Air Quality, Atmosphere & Health (2023) 16:535–551
https://doi.org/10.1007/s11869-022-01287-9

A study on the chemical profile and the derived health effects of heavy-duty machinery aerosol with a focus on the impact of alternative fuels

Nadine Gawlitta[1,2] · Jürgen Orasche[1] · Genna-Leigh Geldenhuys[3,4] · Gert Jakobi[1] · Mark Wattrus[5] · Maximilian Jennerwein[6] · Bernhard Michalke[7] · Thomas Gröger[1] · Patricia Forbes[3] · Ralf Zimmermann[1,2]

Received: 24 May 2022 / Accepted: 17 November 2022 / Published online: 21 December 2022

Abstract

The combustion of petroleum-based fossil fuels is associated with a high environmental burden. Several alternative fuels, including synthetic fuels (e.g., gas-to-liquid, GTL) and biofuels (e.g., rapeseed methyl ester, RME) have been studied in the last few years. While the advantages for the environment (sustainability of biofuels) are well known, research on the resulting health effects from combustion aerosols of these alternative fuels is still scarce. Consequently, we investigated the chemical combustion profile from three distinct fuel types, including a petroleum-based fossil fuel (B0) and two alternative fuels (GTL, RME) under real exposure conditions. We sampled particulate matter ($PM_{2.5}$, $PM_{0.25}$) and the gas phase from heavy-duty machinery and evaluated the general pattern of volatile and semi-volatile organic compounds, elemental and organic carbon as well as a range of transition metals in the size segregated PM and/or gas phase. The use of comprehensive two-dimensional gas chromatography time-of-flight mass spectrometry enabled us to classify distinct methylated PAHs in the PM samples and its high abundance, especially in the fine fraction of PM. We found that (methylated) PAHs were highly abundant in the PM of B0 compared to GTL and RME. Highest concentrations of targeted aromatic species in the gas phase were released from B0. In summary, we demonstrated that GTL and RME combustion released lower amounts of chemical compounds related to adverse health effects, thus, the substitution of petroleum-based fuels could improve air quality for human and the environment.

Keywords Alternative fuels · Combustion aerosol · (methylated) PAHs · Ultrafine particulate matter · Health effects

Introduction

Heavy-duty vehicles are in use on construction sides, in mines, and in other working environments and contribute to a considerable extent to the local air pollution (Traviss et al. 2010; Gautam et al. 2018; Salo et al. 2021). These heavy-duty vehicles are typically powered by fossil fuel. The increasing environmental burden resulting from petroleum-based fossil fuel combustion has led to the ongoing search for alternative fuels (Unosson et al. 2021). Several advantages can be discussed supporting a substitution of petroleum-based fuels by alternative fuels. CO_2 and greenhouse gas (GHG) emissions are lower for alternative fuels compared to petroleum-based fuel combustion (Moon et al. 2010; Zaharin et al. 2017), decreasing the environmental burden, e.g., in terms of its negative impact on climate. Regarding biofuel, several organic feedstocks are available enabling a sustainable way of fuel production. Therefore,

✉ Thomas Gröger
thomas.groeger@helmholtz-muenchen.de

1 Joint Mass Spectrometry Centre (JMSC), Cooperation Group Comprehensive Molecular Analytics, Helmholtz Zentrum München, Neuherberg, Germany

2 Joint Mass Spectrometry Centre (JMSC), Chair of Analytical Chemistry, University of Rostock, Rostock, Germany

3 Department of Chemistry, Faculty of Natural and Agricultural Sciences, University of Pretoria, Pretoria, South Africa

4 Processing Laboratory, Impala Platinum Limited, Rustenburg, South Africa

5 Energy Business, Sasol, Cape Town, South Africa

6 ASG Analytik-Service AG, Neusäß, Germany

7 Research Unit Analytical BioGeoChemistry, Helmholtz Zentrum München, Neuherberg, Germany

biofuels are a prominently discussed alternative to petroleum-based fuels (Traviss et al. 2010; Sakthivel et al. 2018; Unosson et al. 2021). Biofuels can be generated from oil-producing crops, and vegetable oils can be utilized in a pure or transesterified form into biodiesel. Other feedstocks are sugar or starch crops for the production of alcohols such as methanol or ethanol (Yasin et al. 2019). Biofuels from oil-producing crops can be separated in three different generations including vegetable oil (first generation), nonedible vegetable oil (second generation), and waste cooking oil (third generation) (Sakthivel et al. 2018). The chemical and physical properties of a biofuel are mostly dependent on the feedstock. For example, waste cooking oil is a widely used biofuel due to its low cost, but it has inferior cold-flow properties, which limits its use in winter months (Moon et al. 2010). Up to now, biofuels are mostly utilized as diesel–biodiesel blends to overcome difficulties in terms of cold-flow properties as well as long-term negative consequences of the use of pure biofuel such as injector coking, deposits, and ring sticking (Moon et al. 2010). Several studies have been conducted to increase the efficiency of biodiesel use compared to petroleum-derived diesel, but still, contradictory data is available on the emissions of biodiesel combustion and resulting health effects (Bluhm et al. 2012; Møller et al. 2020). A typical feedstock of vegetable oil widely used is rapeseed methyl ester (RME). This fuel is gained by the transesterification of rapeseed oil. RME is primarily composed of fatty acid methyl esters (FAMEs) with different lengths of alkyl chains. As this fuel has no aromatic content, polycyclic aromatic hydrocarbons (PAHs) cannot be emitted by unburned fuel. Another alternative widely discussed in the substitution of petroleum-based fuel is the synthetic gas-to-liquid (GTL) fuel. It is gained by, e.g., the Fischer–Tropsch process from natural gas, leading to a fuel with negligible amounts of aromatic compounds and sulfur (Li et al. 2007; Moon et al. 2010). GTL can usually be used in conventional diesel engines without any engine hardware modifications (Moon et al. 2010). This fuel is primarily composed of long-chain alkanes and, thus, expected to emit lower amounts of PM, in particular, PAHs compared to fossil fuel combustion. Recently, an alternative to the synthetic GTL has gained more attention, the so-called biomass-to-liquid (BTL) fuel, which is produced in a similar way as the GTL after gasification from biomass (van Steen and Claeys 2008).

Generally, fuel combustion releases high quantities of particles. This particulate matter (PM) is physically characterized by its aerodynamic diameter (size distribution) and mass. Only particles with an aerodynamic diameter equal to or smaller than 2.5 µm are expected to deeply penetrate into the respiratory tract (Hussain et al. 2011). The particles themselves and the semi-volatile organic compounds (SVOCs) bound to the particles can be released into the lung leading to acute and inflammatory effects (Salo et al. 2021). Recently, the WHO updated their guidelines in which they suggest even lower maximum exposure levels for $PM_{2.5}$ and other air pollutants due to their known adverse health effects, e.g., the increased risk of respiratory and cardiovascular diseases (Lin et al. 2015; World Health Organization 2021). Moreover, the importance of further characterizing specific PM such as ultrafine particles (UFP) was emphasized (World Health Organization 2021). UFP are particles with an aerodynamic diameter smaller than 0.1 µm. Due to their low size, UFP are physically not restricted to the respiratory tract but can also be translocated to other organs via the bloodstream (Hussain et al. 2011). Moreover, UFP have a high-specific surface area and, thus, vast amounts of organic compounds can be adsorbed onto these particles. The translocation and the intense loading are expected to have adverse health effects and highlight the need for further characterization of UFP (Kwon et al. 2020).

Aerosol from fossil fuel combustion is loaded with a plethora of different chemical components, of which polycyclic aromatic hydrocarbons (PAHs) are of specific health concern. Many PAHs are known to be carcinogenic and mutagenic (Abdel-Shafy and Mansour 2016). Due to their gas-to-particle equilibrium, they can occur particle-bound or in the gas phase. For single compounds, their presence in either of these phases mostly depends on their molecular weight and vapor pressure. For complex samples such as aerosol produced by combustion processes, the gas-to-particle partitioning is mostly influenced by the ambient air temperature and the total organic aerosol concentration (C_{OA}) (Shrivastava et al. 2006). At high C_{OA} and, thus, low dilution ratios the SVOCs are prone to be absorbed into the particle phase (Lipsky and Robinson 2006; Shrivastava et al. 2006). Working environments like construction sites and mines are using vehicles, which emit high amounts of combustion aerosol. During their working shifts, workers may be exposed to high amounts of potentially hazardous air pollutants when operating this kind of heavy-duty machinery. It is, thus, important to gain further insights on the combustion aerosol of distinct fuel types and their possible resulting health effects on employees.

In this study, we focused on the comparison of the chemical profile of the combustion aerosols from three distinct fuel types and their possible health-related effects on workers in a confined working environment. For this purpose, we sampled particles and gas phase of a heavy-duty (Load-Haul-Dump, LHD) vehicle fueled with petroleum-derived fossil fuel (B0), GTL, and RME in a South African platinum mine (1000 m underground). As ventilation may be insufficient and space limited, occupational exposure to combustion aerosols in mining environments is of specific concern (Salo et al. 2021). We aimed at comparing the exposure profile of the currently used diesel fuel to the alternative fuels (GTL,

RME) to enable a comprehensive characterization of the chemical compounds emitted and to estimate their possible health-related effects. Combustion aerosol of the three fuel types was sampled in terms of $PM_{2.5}$, size-segregated PM with an emphasis on $PM_{0.25}$, and the gas phase.

The analysis of PM samples focused on the chemical characterization of substituted and unsubstituted PAHs in the combustion aerosol of the different fuel types, and a comparative analysis of the different size fractions. We also investigated alkylated PAHs were classified based on their aromatic core and methylation pattern. Moreover, concentrations of seven distinct unsubstituted PAHs (phenanthrene, anthracene, fluoranthene, pyrene, benz(a)anthracene, benz(e)pyrene, benz(a)pyrene) were calculated, and toxic equivalents (TEQs) were determined. Additionally, the elemental composition of the PM samples regarding transition metals, alkaline metals, and other elements was performed and compared between the different combustion aerosols. The worker exposure to the gas phase was compared between B0, GTL, and RME highlighting their differences in aromatic carbon content. In particular, concentrations of benzene, toluene, o-xylene, naphthalene, and biphenyl were calculated and compared for the gas phase of the different combustion aerosols. Finally, the gaseous organic compounds, mainly volatile organic compounds (VOCs), were collected in two distinct sampling positions (engine operator and tailpipe), enabling a more comprehensive comparison of concentrations workers could be exposed to during working procedures.

Experimental section

Sampling site

Aerosol sampling was conducted in a platinum mine in South Africa 1000 m underground. The heavy-duty vehicle used in this sampling campaign was a load-haul-dump (LHD) vehicle typically used in this underground mine. The sampling station was 1.5 m from the tailpipe (TP) as well as 1 m above ground (Fig. 1a).

The following samples have been taken: $PM_{2.5}$, size-segregated PM (Sioutas, $n=3$), gas phase during test cycle (TeC), and gas phase in high idling (HI) mode of the LHD (Fig. 1b). Gas phase samples were additionally taken at the LHD operator position (OP) at human chest height during TeC and in HI mode (Fig. 1a). The complete sample set and the conducted chemical analysis are summarized in Table 1.

Engine operations

The LHD was equipped with a Deutz BF 6L 914C engine. Engine specifications are summarized in following Table 2.

The LHD was filled with the specific fuel type at the beginning of each sampling day. For that purpose, the remaining fuel was drained from the LHD, fuel filters and air filters were exchanged and the tank was flushed with 20 L of the test fuel before filling the tank. Lubrication oil was exchanged prior sampling. Afterwards, the LHD returned to work in production for 30 min before returning to the test site. For aerosol sampling, the LHD vehicle was parked at the common parking area of those vehicles at which the sampling was conducted without movement. A pre-conditioning cycle was performed for 10 min to ensure temperature

Table 1 Summary of samples taken and analysis carried out. *EC* elemental carbon, *OC* organic carbon

	B0	GTL	RME
PM analysis			
EC/OC	$PM_{2.5}$, $PM_{0.25}$	$PM_{2.5}$, $PM_{0.25}$	$PM_{2.5}$, $PM_{0.25}$
Elements by ICP-AES	$PM_{2.5}$, $PM_{0.25}$	$PM_{2.5}$, $PM_{0.25}$	$PM_{2.5}$, $PM_{0.25}$
SVOC by GC × GC–MS	$PM_{2.5}$, $PM_{0.25}$, size-segregated PM	$PM_{2.5}$, $PM_{0.25}$	$PM_{2.5}$, $PM_{0.25}$
Gas phase analysis			
VOC by GC–MS	TP (TeC, HI)	TP (TeC, HI)	TP (TeC, HI)
VOC by GC–MS	OP (TeC, HI)	OP (TeC, HI)	OP (TeC, HI)

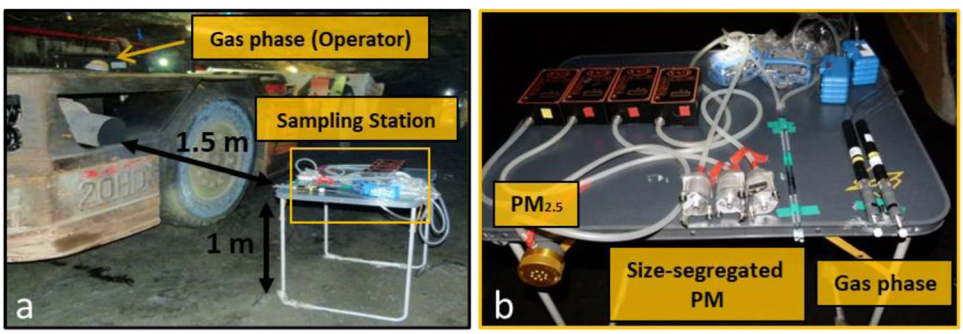

Fig. 1 Underground sampling site of combustion aerosols. Sampling station and additional gas phase sampling at the operator are depicted (**a**). Main sampling station. Samples taken from left to right (**b**): $PM_{2.5}$, size-segregated PM, and gas phase

Table 2 Engine specifications of a Deutz BF 6L 914C engine

Emission certification	Tier 2
No. of cylinders	6
Bore/stroke	102/132 mm
Displacement	6.5 L
Compression ratio	18
Stroke	132 mm
Rated power	141 kW (herein de-rated to 118 kW)
Max. torque	700 Nm at 1600 rpm
Induction	Charged air cooled
Fuel injection	Five-hole nozzle injection; high pressure in-line injector pump with mechanical centrifugal governor
Specific fuel consumption	210 g $(kWh)^{-1}$

stabilization prior aerosol sampling. Aerosol sampling was conducted in 10-min intervals in the two modes. High idling (HI) was conducted with full acceleration and 0% throttle. The test cycle (TC) was done including a bucket lift with a fixed mass (one tire) which should mimic a load test. More information on engine operations by LHD vehicles can be found in Wattrus et al. (2016).

Fuel types

Three different fuels were used for sampling of the corresponding combustion aerosol: (1) a petroleum-derived diesel fuel with no biofuel content (B0), representing the reference diesel used in the working place, (2) a paraffinic fuel (GTL, ORYX, Qatar) compatible with EN15940, and (3) a biofuel (RME, SBE BioEnergie, Germany) according to EN14214 additivized with oxidation stabilizer. The organic composition of B0 and lubrication oil used in this study was characterized by GC × GC-ToFMS and the elemental composition of lubrication oil was also determined by ASG Analytik-Service AG. Fuel properties and composition of GTL and RME were analyzed by Sasol Limited. Further information on the composition and properties of fuel and lubrication oil used can be found in Tables S1–S6.

Sampling and analysis of PM

PM was sampled on quartz fiber filters (QFF) (Quartz-Microfibre Discs, Ahlstrom-Munksjö, Finland) with a deployable particulate sampler (DPS) (SKC Inc., USA) and a cut-off of 2.5 µm. These $PM_{2.5}$ samples were continuously sampled for all three fuel types during TeC and HI mode at a flow of 10 L min^{-1} for 21 min in total. In a similar manner, size-segregated PM was sampled with a Sioutas five-stage cascade impactor (SKC Inc., USA) at a flow of 9 L min^{-1} for 21 min. The five size ranges include > 2.5, 2.5–1.0, 1.0–0.5. 0.5–0.25 and < 0.25 µm. Samples were collected on a 25-mm QFF on the different stages and on a 37-mm QFF (Quartz-Microfibre Discs, Ahlstrom-Munksjö, Finland) on an after-filter (< 0.25 µm). PM samples were taken at the main sampling station solely (Fig. 1). Three experimental replicates were taken for the size-segregated samples for every fuel type (Fig. 1b). Filter samples were kept in the corresponding samplers for transport until filter exchange could be carried out under clean surrounding conditions at the same day. Samples were stored at − 20 °C until analysis.

PM samples were prepared on the day of analysis. QFF were cut by defined punches ($d = 2$ mm) and placed into glass inserts for the direct thermal desorption unit for analysis. These glass inserts were deactivated with trimethylchlorosilane (TMCS, Fisher Scientific, Germany) prior use. The analyzed filter corresponded to 1.64×10^{-2} m^3 for the stages, 7.47×10^{-4} m^3 for $PM_{0.25}$ and 8.10×10^{-4} m^3 for $PM_{2.5}$ samples of collected aerosol. 1 µL of an internal standard (ISTD) was applied to the QFFs by an autosampler (PAL 3 DHR, CTC Dual Head) prior to analysis (see Table S7 for ISTD).

Determination of SVOC on PM was conducted on a direct thermal desorption (DTD) comprehensive two-dimensional gas chromatography (GC × GC) time-of-flight mass spectrometer (ToF–MS, Pegasus BT 4D, LECO, USA). An OPTIC-4 inlet system (GL Sciences, Netherlands) was used. The GC column setup was as follows: A BPX5 capillary column (60 m, 0.25 mm i.d., 0.25 µm d_f, SGE, Australia) was installed as the first dimension and a BPX50 capillary column (1.4 m, 0.1 mm i.d., 0.1 µm d_f, SGE, Australia) was installed as the second dimension. A BPX5 capillary column (2 m, 0.25 mm i.d., 0.25 µm d_f, SGE, Australia) was additionally installed as a pre-column. A temperature gradient of 2 °C min^{-1} in the temperature range of 40 to 330 °C was applied for GC analysis. More detailed information on the applied methodology for thermal desorption and gas chromatographic separation can be found in Tables S7–S9. The MS transfer line and ion source temperature were set to 300 °C and 250 °C, respectively. The mass acquisition was from 35 to 700 Da at an acquisition rate of 100 spectra/s. The electron energy applied was 70 eV.

Data acquisition and processing were carried out using the ChromaTOF software (Version 5.5, LECO, USA). Peak finding was conducted for the complete run with a signal-to-noise (S/N) set to 300. Total ion chromatogram (TIC) was used as a quantitation signal. The spectral match required for peak combination was 800. The spectral similarity was compared with the National Institute of Standards and Technology (NIST) library (version 2.3, 2017). The mass range compared for library search was 35 to 600 m/z. The relative abundance threshold was set to 10. The minimum similarity for matches was set to 700 before the hit was assigned. For the classification of alkylated PAHs, distinct retention time regions were marked and spectral filters specific to those PAHs were assigned. Unsubstituted PAHs were targeted using their molecular mass ion and their elution on the selected column with respect to their deuterated standard. Internal standards were applied for quantification (Table S10).

We applied ChromaToF Tile (version 0.27.2.0, Leco, USA) to perform a comparative analysis of the SVOC pattern of $PM_{0.25}$ samples. Supervised principal component analysis (ANOVA-PCA) was conducted. A *p*-value of 0.05 was used for data comparison. F-ratios were calculated for the significant compounds. Only compounds with an average F-ratio larger than 100 were included in the PCA analysis. Additionally, we excluded the region (RT1: 8000–9000 s and RT2: 1.40–1.87 s) resulting from the column bleed of the instrument. More information on the comparison of the $PM_{0.25}$ by ChromaTOF Tile can be found in the supplementary material (Table S11).

EC and OC contents were determined from the QFFs using a thermal–optical carbon analyzer (Desert Research Institute Model 2001A, Atmoslytic Inc., USA). The analysis was conducted following the IMPROVE_A protocol (Chow et al. 2007).

Elements were determined from the QFFs by inductively coupled plasma atomic emission spectroscopy (ICP-AES; Optima 7300 DV, Perkin Elmer, Germany). Samples were transferred into closed quartz vessels and digested with HNO_3 in a microwave system (Multiwave 300, Anton Paar, Austria). Afterwards, the solution was diluted to 30 mL with ultrapure H_2O. The following elements were determined from the emission samples: Al, As, B, Ba, Be, Bi, Ca, Cd, Co, Cr, Cu, Fe, Hg, K, Li, Mg, Mn, Mo, Na, Ni, P, Pb, S, Sb, Se, Sn, Sr, Ti, V, W, and Zn. Samples were introduced to the system with a peristaltic pump, connected to a micromist nebulizer and a cyclone spray chamber. The power of the radio frequency generator was set to 1400 W. Flow rate of the argon plasma gas and the argon nebulizer gas was 15 L min^{-1} and 0.6 L min^{-1}, respectively. Three blank measurements and one control measurement of a certified standard (CPI, USA) were performed for all elements mentioned previously. Results were calculated with a computerized lab-data management system using calibration curves, blank determinations, and control standards.

Sampling and analysis of gas phase

The gas phase was sampled for all three fuel types. Samples were taken at the tailpipe (main sampling station, Fig. 1) and at the operator during the test cycle (TeC) and in the idle mode of the heavy-duty vehicle. Samples were taken at a flow of 0.5 L min^{-1} for approximately 5 min each. Additionally, the gas phase was taken at the operator during the test cycle as well as idle mode. Flow and sampling time corresponded to the gas phase samples taken at the main sampling station. Adsorber tubes were sampled with Gilian GilAir Plus Personal Sampling Pumps (Gilian, USA). A filter holder assembly made of stainless steel and equipped with a QFF was used for removing the particulate fraction and for protecting the adsorbers. Adsorber tubes consisted of three sublayers of graphitized carbon black (GCB) sorbents used to trap compounds of several volatility ranges (Table S12). At least one adsorber tube was kept closed and taken as field blank for every sampling day. Samples were stored at − 20 °C until analysis.

The analysis of the adsorber tubes was done by thermal desorption (TD) with a Shimadzu TD-20 thermal desorption unit (Shimadzu, Japan), coupled to a GC–MS System (Shimadzu GCMS-QP2010 Ultra, Shimadzu, Japan). The analysis was done according to Mason et al. (2020), but modified to the applied GCB adsorbent material. An isotope-labelled standard mixture was applied to the sample prior to analysis (Table S13). The thermal desorption was performed at 345 °C and lasted 45 min. Extracted compounds were at first concentrated on a Tenax TD trap, cooled at 5 °C, and then redesorbed at 330 °C and transferred with a split ratio of 10 to the gas chromatograph. Separation was done on a 30-m-long VF-xMS, high arylene-modified phase column (0.25 mm ID × 0.25 µm d_f, Agilent Varian, USA). Further information on the temperature program of GC analysis and mass spectral parameters can be found in Table S14.

Raw data files were imported to OpenChrom (Lablicate, Edition 1.4.0.202110221400) as *cdf-files. Peak detection, integration, and identification were applied (Table S15). The 30 most abundant and reliable identified compounds found in the gas phase of the different fuel combustion aerosols were compared. An S/N ratio of 50 was applied as the threshold. Visual sample comparison as well as peak table comparison have been applied. The comparison was based on retention time and mass spectra. Identification was based on mass spectral comparison with the NIST library (version 2.3, 2017). Distinct aromatic compounds have been targeted and semi-quantified by the equivalent isotope-labelled standard compound (Table S13).

Results and discussion

Fuels

In this study, three different fuel types were investigated namely B0, GTL, and RME. B0 represented the petroleum-based reference fuel, that is usually used for the heavy-duty machinery in this platinum mine. GC × GC analysis of this reference fuel revealed dinaphthenes/olefins (22.1%), naphthenes/olefins (21.8%), and iso-paraffins (21.4%) as the most abundant compound classes found in the B0, followed by n-paraffins (16.0%), alkylbenzenes (7.8%), and naphthenobenzenes (6.1%, Table S10). These compound classes make up over 95% of the fuel composition. The remaining 5% can be attributed to indenes (1.6%), naphthalenes (1.6%), and several other aromatic compounds (~ 1.7%, Table S1). GTL and RME were chosen as alternative fuels. The production process for GTL results in a paraffinic fuel mostly consisting of n-alkanes (51.9%) and iso-alkanes (47.7%), making up over 99% of the fuel composition. (The GTL used in this study was produced from natural gas.) Relative amounts of compound classes were determined by GC × GC (Table S1). Only 0.2% of monocyclic as well as 0.2% of bi-and polycyclic paraffins were measured in this fuel and no aromatic compounds were detected. The composition of the RME was determined by standardized analysis methods. Its ester content was determined by EN 14103 and confirmed that the RME used is composed of at least 96.5% of FAMEs (Table S1). Moreover, the RME was defined by maximum values for methanol and mono-, di- and triglyceride content (0.2%, 0.7%, 0.2%, 0.2%, respectively). The content of alkaline metals (Na, K) as well as earth alkali metals (Ca, Mg) was required to be below 5.0 mg kg^{-1} for each of these groups (Table S2). For all three fuel types, distinct properties were determined using standardized analysis methods (ASTM, DIN, EN, ISO). These properties included among others the sulfur content, density, viscosity at 40 °C, flash point, and cetane-number of the respective fuel. The specific fuel properties measured can be found in Tables S1–S4.

Additionally, the lubrication oil utilized in this study was analyzed by GC × GC. We found alkanes (61.5%), followed by dinaphthenes/olefins (20.0%) and naphthenes/olefins (12.5%) add up to 94% of its composition. Furthermore, 2.8% of polynaphthenes/olefins, 1.9% of 2,6-ditert-butylphenole, and 0.5% of benzenes were detected (Table S5). The elemental composition was measured by ICP-AES. We found that the main elements of the lubrication oil were calcium (Ca, 1710 mg kg^{-1}), zinc (Zn, 1300 mg kg^{-1}), and phosphorus (P, 1230 mg kg^{-1}, Table S6). These are typical additives used in lubrication oil (Selby et al. 2005; Lin et al. 2015). Ca is commonly used as a detergent additive, while Zn and P are used as extreme pressure-additives as well as wear protection additives (Selby et al. 2005; Lin et al. 2015). Other abundant elements found in the lubrication oil were boron (B, 310 mg kg^{-1}), followed by sodium (Na, 47.6 mg kg^{-1}), silver (Ag, 11.6 mg kg^{-1}), magnesium (Mg, 8.9 mg kg^{-1}), potassium (K, 8.1 mg kg^{-1}), copper (Cu, 6.8 mg kg^{-1}), and silicon (Si, 5.0 mg kg^{-1}) (Table S15). Na can originate from the anti-corrosion agent $NaNO_2$, Mg is a known detergent additive and Cu is an additive used in high-temperature lubricant (Lin et al. 2015).

Particulate matter

The particulate matter (PM) in the exposure profile derived from the combustion aerosols of LHDs has been chemically characterized. To enable a comprehensive comparison, different techniques to determine the EC/OC ratio, elemental composition, and semi-volatile organic compounds have been applied. Table S16 shows the differences in total, elemental, and organic carbon (TC, EC, OC) content for the PM of the combustion aerosols. $PM_{2.5}$ and $PM_{0.25}$ samples have been analyzed. We found the EC/OC ratio of B0 compared to GTL was similar for $PM_{2.5}$ (0.45 and 0.44, respectively) and $PM_{0.25}$ (0.52 and 0.58, respectively). RME showed a four to five times lower EC/OC ratio (0.11) for $PM_{2.5}$ and $PM_{0.25}$ compared to B0 and GTL. Data recently published by Unosson et al. confirm lower EC/OC ratios for RME compared to B0 (Unosson et al. 2021). Although EC/OC is less for RME PM compared to B0 PM, we found similar TC values. This can be explained by higher OC content for RME compared to B0 PM (Table S16, Fig. 2). These results are consistent with other studies, where lower amounts of EC and higher amounts of OC were found for biodiesel PM compared to PM from fossil fuel combustion due to the higher oxygen content in biodiesel (Lu et al. 2012). Lowest TC and OC were measured for GTL (1.9 mg m^{-3} and 1.2 mg m^{-3}, respectively, Table S16, Fig. 2). This can also be explained by the composition of the fuel as aromatic species and sulfur content are substantially lower compared to B0 fuel. These differences in the carbon content of the PM can be derived from the composition of the distinct fuel types. The different fractions of OC and EC content for $PM_{2.5}$ and $PM_{0.25}$ for all three fuels can be observed in Fig. 2.

The comparison of the distinct OC fractions indicated that the first OC fraction (OC1) differs the most from one fuel to another independent from the size fraction of the PM. OC1 reflects thermally desorbed carbon up to a temperature of 140 °C, thus, mainly VOCs are desorbed in this organic fraction (Chow et al. 2007). However, this fraction is also particularly susceptible to incorrect storage and handling of the sample material. The OC2 and OC3 fractions (up

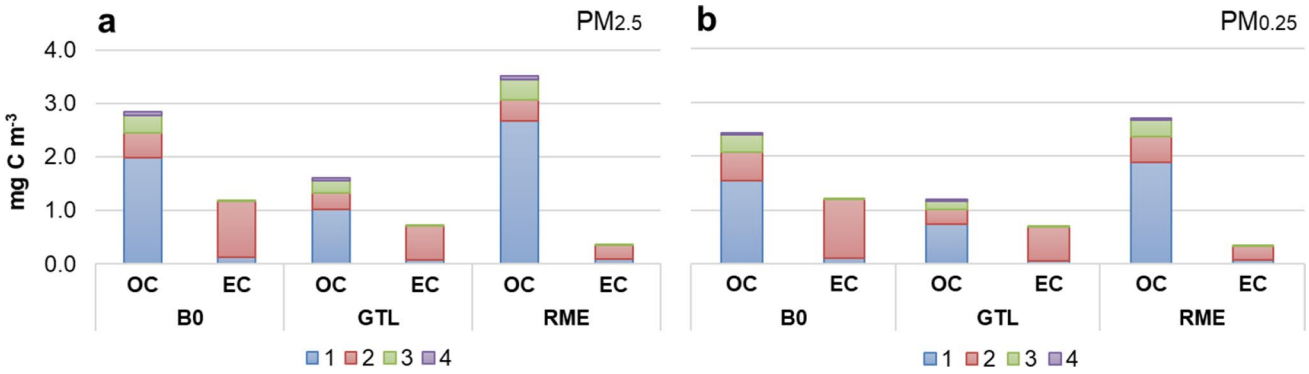

Fig. 2 Determination of the EC/OC-content of the combustion aerosols of the three distinct fuel types (B0, GTL, RME) by a thermal-optical carbon analyzer. OC and EC contents are divided in their distinct fractions. The numbers 1, 2, 3, and 4 represent the respective OC and EC fractions. Data was normalized by m^3. **a** EC/OC content of $PM_{2.5}$ samples is displayed. **b** EC/OC content of $PM_{0.25}$ samples is displayed

to 280 °C and 480 °C, respectively) are characteristic of the desorption of SVOCs (Chow et al. 2007). Additionally, pyrolysis products from compounds with higher molecular weight can be found in OC3 (Diab et al. 2015). Diab et al. demonstrated that the OC2 fraction was mainly composed of PAHs and alkylated PAHs (Diab et al. 2015). As PAHs are intensively discussed in the literature to induce adverse health effects, with some of them being known as potential carcinogens and mutagens and fossil fuel combustion is known to emit high amounts of these hazardous compounds (Boström et al. 2002; Kumar et al. 2014; Sun et al. 2014), we further focused on the analysis of PAHs.

Up to now, the potential toxicity of a sample is mostly conducted by the analysis of the 16 EPA PAHs. These EPA PAHs were selected back in 1976 when knowledge on PAH occurrence and the availability of standard material for identification and quantification purposes was limited (Andersson and Achten 2015). Nowadays, increasing research has been directed to the analysis of different PAH species including alkylated PAHs. Alkylated PAHs are highly abundant in crude oil products and dominate petrogenic sources (Czech et al. 2017). Although pyrogenic sources are dominated by their unsubstituted analogues, the abundance of alkylated PAHs due to unburned fuel as well as combustion processes cannot be neglected. Nevertheless, research on their potential toxicity in comparison to their unsubstituted analogues is still limited. Lam et al. focused on the comparison of the potency and aryl hydrogen receptor (AhR) activation of methylated PAHs compared to their unsubstituted analogues (Lam et al. 2018). They found that the relative potency factors (REPs) of monomethylated PAHs decreased faster than the ones of their parent compounds or other derivatives with increasing exposure time (Lam et al. 2018). This is in agreement with the study of Kang et al. showing a higher solubility of methylated PAHs and thus a higher biotransformation of the incorporated compounds (Kang et al. 2016). This can lead to higher excretion and detoxification of those compounds. Nevertheless, when comparing REPs of chrysene, benz(a)anthracene, and benzo(a)pyrene with their methylated analogues, significantly higher potencies were determined for their methylated analogues. Moreover, they presented higher potencies for PAHs with a methyl group attached to the core compared to ethyl, hydroxyl, and methoxy groups after 24-h exposure duration (Lam et al. 2018). The relative potency determined by the H4IIE-luc assay was, independent of the position of the methyl group attached to the PAH, higher compared to the unsubstituted PAHs (Lam et al. 2018). These studies emphasize the importance of monitoring methylated PAHs in a similar manner as unsubstituted PAHs. We, thus, focused on the classification of methylated three- and four-ring aromatics in the combustion aerosols by comprehensive GC × GC-ToFMS analysis in addition to the unsubstituted PAHs.

For B0, the overall PAH distribution in the samples was similar independent of the particle size (Figs. S1, 3). Most PAHs identified were three- and four-ring aromatics with different methylation patterns (Figs. S1, 3). Three-ring aromatics were found with up to four methyl groups and multiple alkyl groups attached to the ring structure. The abundance of the three-ring aromatics increased with increasing methylation having a maximum at the group of three times methylated (C_3) three-ring aromatics. For three-ring aromatics with higher methylation patterns, the abundance decreased again (Figs. S1, 3). The four-ring aromatics show a decrease in the abundance with an increase of methylation. A maximum of three times methylated four ring aromatics was identified. The abundance of two to four-times methylated three-ring aromatics is higher than the one found for the methylated four-ring aromatics. When comparing these PAH patterns to the literature, we found the distribution of methylated three-ring aromatics (bell-shape) is typical for PAHs originating from unburned fuel (Andersson and Achten 2015). In

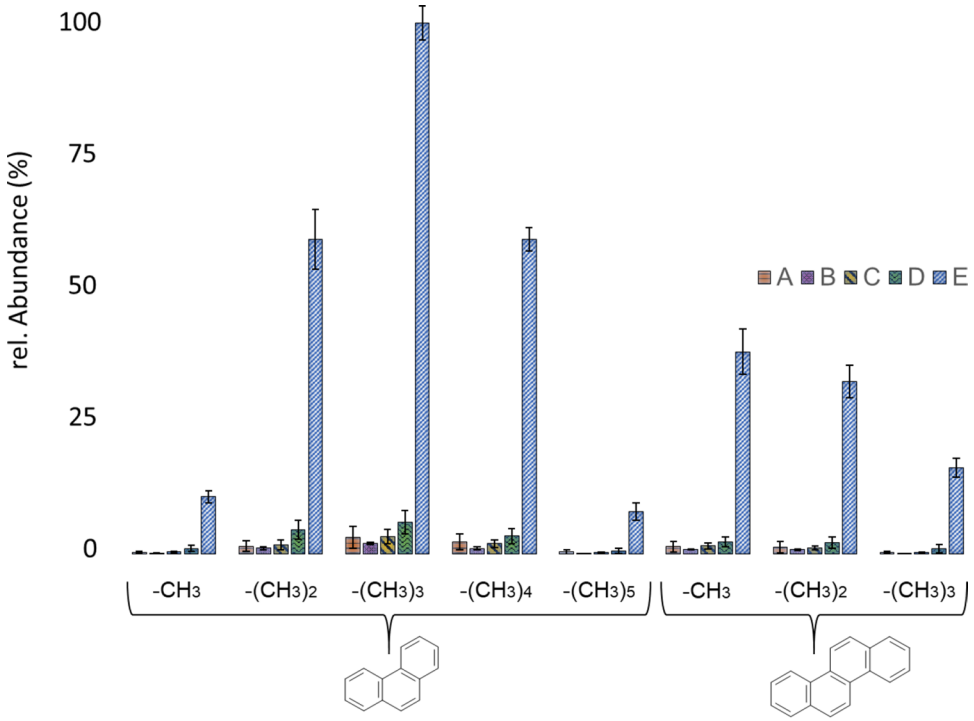

Fig. 3 PAH distribution of B0 for the following particle sizes: A (> 2.5 µm), B (2.5–1.0 µm), C (1.0–0.5 µm), D (0.5–0.25 µm), and after-filter E (< 0.25 µm). Phenanthrene and chrysene are exemplary shown as reference compounds for the three- and four-ring aromatics, respectively. Degree of methylation is shown as the amount of $–CH_3$ groups substituted to the core. The highest abundance of PAHs can be found on the quasi-ultrafine particle after-filter E. Stages and after-filter were simultaneously sampled in triplicates and analyzed via TD-GC × GC-ToFMS. Sample abundance is shown as an area normalized by m^3. Standard deviation is depicted as error bars

contrast, the distribution found for the four-ring aromatics and a lower abundance with an increasing amount of methylation ($C_0 > C_1 > C_2 > C_3 > C_4$) is typical for PAHs arising from the combustion process (Andersson and Achten 2015). In this context, it is important to mention that PAHs can generally originate from three different sources. First, they can originate from unburned fuel or the lubrication oil (Kleeman et al. 2008; Czech et al. 2017). Second, they can be formed by the hydrogen abstraction-C_2H_2 addition (HACA) mechanism (Kislov et al. 2013; Czech et al. 2017). Third, they can be broken down to smaller PAHs by pyrolysis (Diab et al. 2015; Abdel-Shafy and Mansour 2016). In combustion engines, unsubstituted PAHs are noticeably formed by the HACA mechanism. The number of rings formed in this process depends on the combustion temperature. Czech et al. stated that in a homologue series of PAHs, usually the unsubstituted or (mono-) methylated PAH shows the highest abundance, but also higher alkylation degrees are visible especially for larger diesel engines due to a higher release of unburned fuel (Czech et al. 2017).

For the size-segregated PM, we used the Sioutas impactors, which enabled sampling of PM in the following size range: A (> 2.5 µm), B (2.5–1.0 µm), C (1.0–0.5 µm), D (0.5–0.25 µm), and after-filter E (< 0.25 µm). Ultrafine particles are defined as particles with an aerodynamic diameter equal or smaller than 100 nm. Due to the cut-off point of the Sioutas impactors, we could only sample particles with a diameter equal or smaller than 250 nm. Nevertheless, we assume that the collected combustion particles will still mainly be ultrafine particles at this cut-off and, thus, this fraction will be referred to as "quasi"-ultrafine particles (qUFP) throughout the manuscript. We found that the "quasi"-ultrafine particles (qUFP, $PM_{0.25}$, after-filter E) show the highest abundance of PAH compared to all other size ranges (Fig. 3). The PAHs classified on these qUFP represent at least 80% of the PAHs classified on the total PM (Stage A–E). As the majority of PM released from diesel engine combustion is accounted to the ultrafine fraction (in terms of particle number) (Salo et al. 2021), the identification of more than 80% of the classified PAHs on the qUFP is plausible. The analysis of the several size ranges showed higher variances for samples from stages A to D compared to the after-filter (E). Although less pronounced as for the qUFP, we can still observe the typical PAH distribution described previously (Fig. 3 insert).

As the classified PAHs are certainly most abundant on the qUFP and UFP are of specific health concern, we further focused on the composition of the $PM_{0.25}$ samples when comparing the combustion aerosol of B0 to the combustion aerosols of the alternative fuels GTL and RME.

The PAHs classified are noticeably most abundant in the B0 combustion aerosol, followed by GTL and RME (Fig. 4). For most of the PAHs determined, we found that the abundance is at least twice as high in B0 compared to GTL. Multiply alkylated three-ring aromatics and three times methylated four-ring aromatics cannot be identified in GTL. The PAH distribution found for B0 can be confirmed for GTL. We found an increase of PAH abundance up to C_3-PAH for

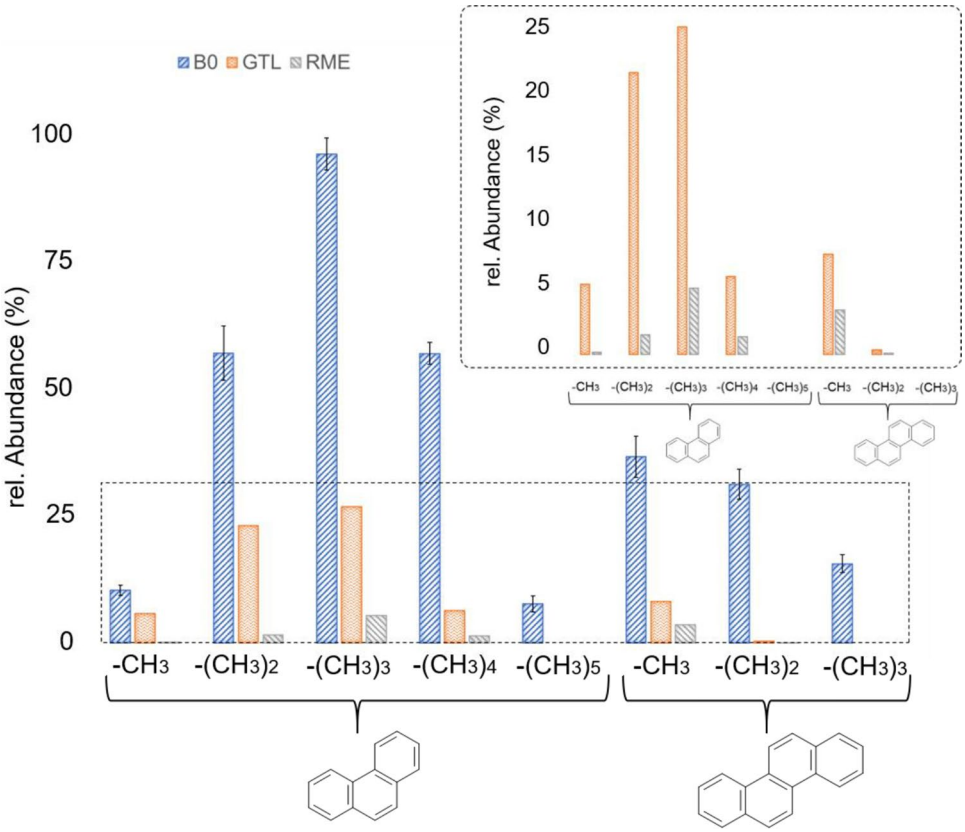

Fig. 4 PAH distribution analyzed from the "quasi"-ultrafine particles ($PM_{0.25}$) for B0, GTL, and RME. Phenanthrene and chrysene are exemplary shown as reference compounds for the three- and four-ring aromatics, respectively. Degree of methylation is shown as the amount of $–CH_3$ groups substituted to the core. B0 was simultaneously sampled in triplicates, whereas GTL and RME can only be shown as two experimental replicates. Sample abundance is shown as the area normalized by m^3 sampled. Standard deviation is depicted as error bars for samples measured in triplicates. Insert: Detailed view of PAH distribution of GTL and RME solely

the three-ring aromatics and a decline of abundance with increasing methylation for the four-ring aromatics.

The amount of PAHs classified in the combustion aerosol of RME is distinctly less compared to B0 and GTL (Fig. 4). The distribution of the PAHs, though, equals the distribution found for GTL and B0 combustion aerosol. The abundance of the PAHs on the RME $PM_{0.25}$ is at least twofold less compared to GTL. We determined an abundance four times lower for the C_3-PAHs group in RME compared to GTL and twelve times lower compared to the B0 $PM_{0.25}$ samples. For the four-ring aromatics, we confirm the decrease of abundance with increasing methylation, which was already observed for B0 and GTL. The groups of multiply alkylated three-ring aromatics and three times methylated four-ring aromatics cannot be identified in the $PM_{0.25}$ samples of RME.

This aspect is important when discussing health aspects of distinct combustion aerosols. The exposure to (alkylated) PAHs is known to have adverse effects on human health. A change in fuel type could, thus, greatly decrease the amount of alkylated PAHs released. Moreover, the confirmation of PAHs mainly found on the qUFP is of great concern as these particles can deeply penetrate into the lung, enter the alveolar region, and can even be translocated to other organs (Hussain et al. 2011). Although they have a low particle mass, UFP have a very high particle number and, thus, a high surface area on which different chemical components can be absorbed or adsorbed onto (Kwon et al. 2020). This is also explaining the high amount of alkylated PAHs (over 80% of total alkylated PAHs classified) found on the $PM_{0.25}$ fraction.

To enable a comparison to previous research results and to give a more comprehensive picture of the chemical profile of the PM from these distinct fuel types, we additionally targeted seven unsubstituted PAHs in the $PM_{0.25}$ of B0, GTL, and RME. We found that, independent of the targeted PAH, the combustion of B0 released highest PAH concentrations compared to GTL and RME. The comparison of GTL and RME combustion aerosol showed higher concentrations of smaller PAHs (phenanthrene, anthracene, fluoranthene, pyrene) for GTL. In contrast, higher molecular weight PAHs (benz(a)anthracene, benz(e)pyrene, benz(a)pyrene) were more prominent in the RME combustion aerosol compared to GTL. The prevalence in the formation of specific PAHs can be explained by the composition of the fuels and the resulting differences in the combustion process. While the paraffinic GTL is mainly consisting of smaller alkane and alkene compounds, which mostly leads to the formation of smaller PAHs by butadiene addition reactions (Kislov et al. 2013), RME mainly consists of FAMEs of different lengths of alkyl chains. As stated by Llamas et al., FAMEs are primarily consumed by the abstraction of the H atoms by OH•and H radicals (Llamas et al. 2017). The

α-hydrogen atom in regard to the ester group is the most labile H atom due to resonance stabilization of the resulting radical. The more stable radical will decompose later to a stable acrylic ester molecule and a ($R\text{-}CH_2\bullet$) radical which can induce a chain reaction by β-elimination. This radical can form several PAH and soot precursor in the flame such as acetylene, ethylene and 1,3-butadiene. Ethylene and 1,3-butadiene could then form benzene, naphthalene, anthracene, and phenanthrene by Diels–Alder reaction followed by aromatization (Llamas et al. 2017). This would explain the detection of smaller PAHs in the RME combustion aerosol. The formation of larger PAHs could be explained by the Diels–Alder reaction of those lighter PAHs and ethylene followed by aromatization of the naphthenic-aromatic hydrocarbon formed. Herein, oxygen would serve as a hydrogen acceptor to produce water in the combustion process (Llamas et al. 2017).

Nisbet and Lagoy proposed toxicity equivalent factors (TEFs) for 16 individual PAHs (Nisbet and Lagoy 1992). These TEFs were based on previously conducted experiments on the toxicity and carcinogenic potential of distinct PAHs compared to the toxic effect of benz(a)pyrene (BaP) and are the basis for the calculation of toxic equivalents (TEQs) for different PM samples. The comparison of the resulting TEQ values shows that the sum of BaP_{TEQ} for the analyzed PAHs is the highest for B0, followed by RME and GTL. The overall higher concentrations of the targeted PAHs in B0, thus, also result in a higher sum of calculated TEQs. Intriguingly, while the concentration of the targeted PAHs is higher in the GTL $PM_{0.25}$, the overall BaP_{TEQ} value is lower compared to RME $PM_{0.25}$ (Table 3). This can be explained by the different TEFs taken into account for the TEQ calculations. Smaller molecular PAHs are known to show lower toxic effects and have, therefore, lower TEFs. This emphasizes the importance of monitoring different PAHs. Especially, higher molecular PAHs such as dibenzo(a,h)anthracene and indeno(123-c,d)pyrene (which were below the limit of quantification in our study) with TEF of 5 and 0.1, respectively (Nisbet and Lagoy 1992), can significantly contribute to the total toxicity induced by PAHs. Moreover, the toxicity of alkylated PAHs should be further investigated to enable an assessment of their potential TEQ values. Recently, Richter-Brockmann and Achten highlighted the importance of alkylated PAHs, in particular 1-methylpyrene and 5-methylchrysene, on the overall toxicity of environmental samples and proposed their consideration in future risk assessments (Richter-Brockmann and Achten 2018). In summary, valuable TEF values for PAH derivatives are needed to achieve a more realistic estimation on the toxicity of complex aerosol samples. Nevertheless, we found higher abundances in the alkylated PAHs as well as higher concentrations of all targeted unsubstituted PAHs in the B0 in comparison to GTL and RME $PM_{0.25}$. Based on this data, the change in fuel type would not only lead to the use of more sustainable energy sources as well as to an independence of fossil fuel supply, but might additionally improve the exposure situation.

As alkylated PAHs showed the lowest abundance in the $PM_{0.25}$ of RME and also targeted PAHs showed lower concentrations compared to B0 $PM_{0.25}$, the higher OC measured for RME must derive from another source. We noted previously that RME consists of high amounts of FAMEs in the fuel (Table S2). To evaluate whether FAMEs contribute to the most distinct differences of PM between RME, GTL, and B0, we performed a supervised analysis of variances-principal component analysis (ANOVA-PCA) of the $PM_{0.25}$ of these three fuels (Fig. S2). A detailed look at the components with the greatest loadings towards the RME samples included FAMEs of various lengths of alkane side chains as being the most significant components (Fig. S3, Table 4). Although this type of statistical analysis cannot state quantitative differences between the samples, Table 4 shows highest areas are clearly measured for the distinct FAMEs, e.g., docosanoic acid methyl ester and tetracosanoic acid methyl ester, in comparison to the other significantly different compounds from RME to GTL and B0 $PM_{0.25}$ samples. This might be an explanation for the higher OC content of RME combustion aerosol compared to GTL and B0. Besides two unknown compounds, we found two cyclic

Table 3 Targeted PAHs in the $PM_{0.25}$ samples of B0, GTL, and RME. TEF values are based on the proposed TEF by Nisbet and Lagoy (Nisbet and Lagoy 1992). TEQ values were calculated by multiplying the concentration of a PAH by its proposed TEF. Concentrations are given in ng m^{-3}

	B0	GTL	RME	TEF	B0 BaP_{TEQ}	GTL BaP_{TEQ}	RME BaP_{TEQ}
Phenanthrene	76.1	48.2	26.6	0.001	0.1	< 0.1	< 0.1
Anthracene	23.1	11.3	n.d	0.01	0.2	0.1	n.d
Fluoranthene	62.9	48.3	33.5	0.001	0.1	< 0.1	< 0.1
Pyrene	237	177.1	118.2	0.001	0.2	0.2	0.1
Benz(a)anthracene	21.5	1.7	13.2	0.1	2.2	0.2	1.3
Benz(e)pyrene	12.1	2.4	7.9	0	0	0	0
Benz(a)pyrene	15.7	0.2	11.6	1	15.7	0.2	11.6
∑	**449**	**289**	**211**		**19**	**0.8**	**13**

n.d. not detected

Table 4 Table content derived from supervised ANOVA-PCA (Figs. S2, S3). Components with highest loadings towards RME from the $PM_{0.25}$-bound combustion aerosol are listed and sorted from highest to lowest abundance. Identification and similarity calculations are based on NIST library hits

Name	Compound class	F-ratio	Abundance rel. (%)	Similarity
Docosanoic acid, methyl ester	FAME	542	100.00	883
Tetracosanoic acid, methyl ester	FAME	354	55.03	908
Methyl 8-(2-furyl)octanoate	Ester	415	12.15	966
15-Tetracosenoic acid, methyl ester	FAME	124	10.16	898
Cyclopentene, 1-butyl-	Naphthene	1904	9.84	957
13-Docosenoic acid, methyl ester, (Z)-	FAME	181	9.32	889
Methyl 10-oxohexadecanoate	Ester	695	6.48	798
cis-Methyl 11-eicosenoate	Ester	969	3.66	874
10-Oxodecanoic acid, methyl ester	FAME	275	2.43	854
Neophytadiene	Diterpene	379	1.94	916
7-Nonynoic acid, methyl ester	FAME	174	1.21	762
11,13-Eicosadienoic acid, methyl ester	FAME	283	0.95	915
Methyl 18-methylnonadecanoate	Ester	1920	0.75	872
Unknown (not identified)	-	630	0.61	-
Methyl 8-(5-hexyl-2-furyl)-octanoate	Ester	172	0.56	855
2-n-Octylfuran	Furan	377	0.40	965
Nonadecanoic acid, methyl ester	FAME	687	0.27	810
Butylated Hydroxytoluene	Phenol derivative	460	0.19	902
Unknown (not identified)	-	164	0.06	-
3-Methylene-7,11-dimethyl-1-dodecene	Alkene	275	0.05	830

compounds (1-butyl-cyclopentene and 2-n-octylfuran), an alkene (3-methylene-7,11-dimethyl-1-dodecene), which is expected to have no influence on the toxicity of the aerosol, a diterpene (neophytadiene) and an aromatic compound (Butylated Hydroxytoluene, BHT). BHT is a known antioxidant and commonly used as an oxidation stabilizer in petroleum products (Ryu 2010). As RME is a biodiesel composed of many polar substances, it is important to ensure the stability of this fuel during use and storage. We, thus, propose that BHT was used as the oxidation stabilizer in this biofuel.

Besides, organic compounds also various metals are considered to have adverse health effects. Therefore, we compared the elemental composition of the ultrafine $PM_{0.25}$ samples from B0, GTL, and RME by ICP-AES. We analyzed a wide range of elements, whereas the most hazardous group of elements measured were the transition metals (Table S17). Cu, Fe, Ni, Ti, and Zn were found in at least one of the combustion aerosols from the distinct fuels. Cu was only detectable in B0 (592 ng m^{-3}), while it was below the limit of quantification (LOQ) for GTL and RME combustion samples. Cu is usually released by wear abrasion. As our sampling approach was conducted without moving of the vehicle, we did not expect significant amounts of copper being present in our samples. As Cu is also used as an additive in high-temperature lubricants and we confirmed Cu in the lubrication oil measured, we expect the Cu found in the B0 combustion aerosol derived from the lubrication oil. Although the lubrication oil was the same for all tested fuel types, the fuel and the resulting combustion temperature can influence the release of unburned lubrication oil. Fe showed the highest concentration in the PM of B0 (7146 ng m^{-3}) compared to GTL and RME (6963 ng m^{-3} and 5918 ng m^{-3}, respectively).

The highest concentration of Ni was determined in the GTL samples (1047 ng m^{-3}) compared to B0 (881 ng m^{-3}) and RME (666 ng m^{-3}). Al showed highest concentrations for GTL (9570 ng m^{-3}) in comparison to B0 and RME (8585 ng m^{-3} and 4413 ng m^{-3}, respectively). The higher concentrations of Ni and Al in the PM of GTL could be explained by the production process of the fuel. Nickel is a commonly used catalyst in the Fischer–Tropsch process and Al_2O_3 is a known support material used, i.e., to enhance the mechanical stability of the catalyst (van Steen et al. 2008). Zn concentration was highest for RME combustion aerosol (5631 ng m^{-3}) compared to B0 (4375 ng m^{-3}) and GTL (1588 ng m^{-3}). Alkali (K, Na) and alkaline earth metals (Ba, Ca, Mg) showed highest concentrations for RME combustion aerosol compared to B0 and GTL (Table S18). The following concentrations were determined for the RME $PM_{0.25}$ samples: K (88 µg m^{-3}), Na (14 µg m^{-3}), Ba (914 ng m^{-3}), Ca (18 µg m^{-3}), and Mg (2206 ng m^{-3}). Mg concentrations were below the LOQ for B0 and GTL. For RME, we found mainly alkali and alkaline earth metals showing the highest abundance compared to the elemental composition of $PM_{0.25}$ of B0 and GTL. The higher concentrations of alkali and alkaline earth metals in the PM of RME could be explained

by their expected occurrence in natural sources such as rapeseed oil and by their common use as catalysts in the transesterification process of biofuels (Arzamendi et al. 2008; Mohadesi et al. 2014; Tavizón-Pozos et al. 2021). Mohadesi et al. studied the catalytic reactivity of alkaline earth metal oxides including CaO/SiO_2, BaO/SiO_2, and MgO/SiO_2 (Mohadesi et al. 2014). Arzamendi et al. studied the catalytic reactivity and selectivity of several alkali and alkaline earth metals in the transesterification process, including among others Na, K, Ca, and Mg carbonites, Na and K bicarbonates, and Ca and Mg oxides (Arzamendi et al. 2008). Recently, Tavizón-Pozos et al. concluded that the combined use of alkaline earth oxides with alkaline metals might enhance their basicity so that more active sites would be available and a higher resistance to environmental factors could be achieved (Tavizón-Pozos et al. 2021). Ti concentrations were comparable between RME and B0 (287 ng m^{-3} and 253 ng m^{-3}, respectively), while it was below the LOQ for GTL $PM_{0.25}$. Sn concentrations were comparable for B0 (221 ng m^{-3}), GTL (208 ng m^{-3}), and RME (215 ng m^{-3}). Non-metals (B, P, S, Se) analyzed were found to be most abundant in B0 combustion aerosol (B, Se) or comparable to RME (P, S) while lowest for GTL (Table S18). Sulfur concentration was measured to be lowest for GTL combustion aerosol (9 µg m^{-3}) which was expected as the fuel is characterized by a low sulfur content (Table S4).

Gas phase

To enable a comprehensive comparison of the complete combustion aerosol produced by the different fuels, the gas phase needs to be considered. As previously mentioned, VOCs and SVOCs are present in an equilibrium between the gas and particulate phase. Their gas-to-particle partitioning is depending on the exhaust temperature as well as the complete organic aerosol concentration (C_{OA}). The identification of VOCs and SVOCs in the gas phase was achieved using TD-GC–MS.

For the comparison of the gas phase from the distinct fuel types, we focused on the samples taken at the tailpipe during the test cycle. Differences in the SVOC and VOC composition of the gas phase between B0, GTL, and RME were assessed. We identified 164 different volatiles in B0 and in GTL and 100 volatiles in the RME gas phase with similar pre-processing conditions. We found that of the 30 most abundant compounds identified in the B0 gas phase, 25 can also be found in the GTL and 26 in the RME gas phase (Table 5). Aromatic compounds like xylene and other methylated benzene isomers are more abundant in the B0 gas phase, while alkanes can be found several orders of magnitude higher in GTL compared to B0 and RME gas phase (Table 5, Fig. S4). This resembles the results already gained by the chemical analysis of the PM samples. The higher abundance of the aromatic species in the B0 gas phase compared to GTL and RME can again be explained by the differences in their fuel composition. The higher amount of aromatic hydrocarbons in the B0 fuel, leads to higher amounts of smaller aromatic compounds by pyrolysis of larger PAHs during the combustion process. The increased amount of alkanes in the GTL gas phase reflects the high abundance of n- and iso-paraffins in this fuel.

To consider whether other chemical compounds were highly abundant in GTL and RME but not found in the B0, we additionally summarized the 30 most abundant compounds found in GTL and RME gas phase (Table S18). The analysis confirmed that the GTL gas phase mainly consists of highly abundant alkane peaks. Most of the components found in the RME gas phase showed smaller abundances compared to GTL and B0, as can already be observed in Table 5. Besides alkanes and aromatic compounds, the presence of FAMEs in the RME gas phase could be confirmed (Table S18).

The gas phase samples evaluated in the previous chapter considered only the sampling of volatiles at TP during TeC. To study in which extent the LHD operator is exposed to volatiles, known to have adverse health effects, we targeted distinct aromatic compounds and included different exposure scenarios which were addressed by our experimental design. Absolute concentrations were determined by equivalent isotope-labeled ISTDs.

The three main parameters for the exposure were as follows: (1) use of different fuels, (2) engine conditions, and (3) sampling position. First, we found that the concentration of the targeted mono- and diaromatic hydrocarbons in the gas phase of the three fuels was observed to be highest for B0 (Table 6). Second, the concentrations calculated during TeC and HI were higher during TeC for most of the compounds independent of fuel type and sampling position. Third, the concentrations measured at the main sampling position (TP) were found to be several times higher for most of the targeted compounds (except for toluene) in comparison to the OP sampling position.

The influence of the different fuel types will exemplarily be discussed for the TeC conditions at the tailpipe (TP). For benzene, we determined a concentration of 311 µg m^{-3} for B0 in comparison to 286 µg m^{-3} for GTL and 210 µg m^{-3} for RME in the gas phase. Toluene concentrations could only be determined for B0 (103 µg m^{-3}) and RME (87.8 µg m^{-3}), as the isotope-labelled standard (toluene-d8) and, thus, the native toluene peak are co-eluting with a highly abundant alkane peak in the GTL samples. O-xylene could only be determined in the B0 gas phase with a concentration of 153 µg m^{-3}. Naphthalene concentrations were similar for B0 (19.5 µg m^{-3}) and GTL (22.7 µg m^{-3}) but four times less in RME (3.78 µg m^{-3}). Biphenyl showed the lowest amount calculated for the targeted gas phase compounds for all fuel

Table 5 Table based on the 30 most abundant peaks found in the gas phase of the B0 during test cycle at the tailpipe. Retention time (RT) and mass spectra similarity was used for component identification

Compound	Peak no.[1]	Class	Rel. Abundance[2] (%)		
			B0	GTL	RME
Benzene	1	Aromatic	48.05	4.92	100.00
Undecane	20	Alkane	100.00	82.10	26.90
Decane	12	Alkane	100.00	100.00	31.94
Dodecane	26	Alkane	73.00	33.11	15.32
Nonane	5	Alkane	43.02	85.23	24.31
Toluene	2	Aromatic	37.99	-[3]	76.21
Tridecane	29	Alkane	37.99	21.10	4.80
Mesitylene	13	Aromatic	35.70	2.17	3.33
p-Xylene	4	Aromatic	25.40	0.83	9.96
Decane, 4-methyl-	14	Alkane	24.49	2.53	3.39
Tetradecane	30	Alkane	23.11	6.13	23.23
Benzene, 1,2,3-trimethyl-	15	Aromatic	20.98	-	1.08
Undecane, 3-methyl-	25	Alkane	20.09	9.13	2.09
Undecane, 2-methyl-	24	Alkane	19.77	10.20	3.36
Nonane, 3-methyl-	9	Alkane	19.08	9.44	1.56
Decane, 5-methyl-	17	Alkane	17.73	8.61	3.86
Undecane, 2,6-dimethyl-	27	Alkane	16.32	1.98	0.62
9-Octadecen-1-ol, (Z)-	19	Alcohol	16.18	-	1.44
Nonane, 2-methyl-	8	Alkane	15.56	8.37	1.93
Decane, 4-methyl-	18	Alkane	14.74	9.04	2.15
Tetradecane, 2,6,10-trimethyl-	28	Alkane	14.28	1.15	4.23
Benzene, 1-ethyl-3-methyl-	10	Aromatic	13.50	0.18	0.92
Cyclohexane, butyl-	16	Naphthene	12.65	0.55	-
trans-Decalin, 2-methyl-	22	Naphthene	12.59	0.25	-
Octane, 4-methyl-	3	Alkane	12.56	9.44	7.18
o-Xylene	6	Aromatic	12.27	-	-
Octane, 2,6-dimethyl-	7	Alkane	12.01	1.58	-
trans-Decalin, 2-methyl-	21	Naphthene	11.95	0.47	1.36
Undecane, 5-methyl-	23	Alkane	11.74	8.37	1.33
Benzene, 1-ethyl-3-methyl-	11	Aromatic	11.53	-	1.63

[1]Peak no.: the numbering of the peaks refers to the statistical analysis (Fig. S4)

[2]Relative abundance was calculated based on the area using TIC

[3]Toluene-d8 is coeluting with a highly abundant alkane peak and, thus, native toluene might not be detectable

types. As biphenyl could not be determined for the TP-TeC condition for GTL, we compared the TP-HI concentrations for B0, GTL, and RME. The concentration of biphenyl found in B0 gas phase (1.08 µg m^{-3}) was twice as high compared to GTL (0.432 µg m^{-3}) and RME (0.558 µg m^{-3}).

The comparison of the different engine conditions (TeC, HI) showed higher compound concentrations during TeC for benzene, o-xylene, and naphthalene for GTL and RME (Table 6). The concentrations for toluene and naphthalene were comparable between TeC and HI in the B0 gas phase at the TP position. The concentration of biphenyl was higher during HI than during TeC at the TP but not at the OP position. As concentrations of the targeted compounds were up to 23 times lower for the OP compared to the TP sampling site (e.g. O-xylene in B0 samples), we expect mainly dilution factors being responsible for this decrease. Although, we were able to confirm dilution effects due to the distance of the OP compared to the TP for the targeted compounds (except for toluene), we were still able to measure concentrations as high as 55.7 µg m^{-3} for benzene and 13.7 µg m^{-3} for o-xylene in the B0 gas phase. Concentrations of naphthalene and biphenyl were 0.535 µg m^{-3} and 0.245 µg m^{-3} at maximum at the OP.

As VOCs have a relatively high vapour pressure, their main exposure pathway is through inhalation. Benzene, toluene, and xylene (BTX) compounds have high potential for

Table 6 Targeted aromatic hydrocarbons in the gas phase samples of B0, GTL, and RME are summarized. Samples were taken at the tailpipe and at the operator level during test cycle and at high idling conditions. Concentrations were normalized to sampling volume in m^3. Single measurements are listed if not stated differently

	Benzene (µg m^{-3})	Toluene (µg m^{-3})	o-Xylene (µg m^{-3})	Naphthalene (µg m^{-3})	Biphenyl (µg m^{-3})
B0					
TP-TeC[1]	311	103	153	19.5	0.648
TP-HI[1]	226	108	115	21.2	1.08
OP-TeC	55.7	-	6.61	0.535	0.245
OP-HI	56.8	95.5	13.7	0.314	0.168
GTL					
TP-TeC	286	-[2]	-	22.7	-
TP-HI	138	-[2]	-	11.9	0.432
OP-TeC	-	-[2]	-	0.465	0.121
OP-HI	40.6	-[2]	-	0.395	0.079
RME					
TP-TeC	210	87.8	-	3.78	0.197
TP-HI	118	84.2	-	1.19	0.558
OP-TeC	7.10	15.8	-	0.294	-
OP-HI	-	-	-	0.185	0.128

[1]Mean values ($n = 2$) are depicted

[2]Toluene-d8 is coeluting with a highly abundant alkane peak and, thus, native toluene might not be detectable

TP tailpipe, *OP* operator, *TeC* test cycle, *HI* high idling

bioaccumulation and are implicated in cancer and tumour cases in humans (Kuranchie et al. 2019). Acute effects of BTX exposure could include eye, nose, and skin irritation as well as headaches, tiredness, and dizziness. A chronic exposure to these VOCs could consequently pose a risk for cancer as well as it could damage liver, kidneys, heart, lungs, and other organs (Kuranchie et al. 2019). Benzene is the most toxic component and has been confirmed to be carcinogenic to humans (group 1) by the US EPA (Kuranchie et al. 2019; Mihajlović et al. 2021). After inhalation, benzene is converted to toxic metabolites and can produces mutagenic properties (Kuranchie et al. 2019).Toluene is known to induce skin and eye irritations and operates depressant on the central nervous system (CNS). Xylenes are irritants for the eye, skin, and mucous membrane and can cause among others respiratory and gastrointestinal damage (Kuranchie et al. 2019). Naphthalene has been categorized as possibly carcinogenic to humans (group 2B) by the International Agency for Research on Cancer (IARC) (Yost et al. 2021). While epidemiological studies are limited to two occupational exposure studies which demonstrated limited evidence for effects on the nervous system of the workers by exposure to biphenyl above the occupational threshold limit value (1.3 mg m^{-3}), experimental animal studies of ingested biphenyl provided consistent evidence for renal and some evidence for liver toxicity (Li et al. 2016). Moreover, carcinogenicity of biphenyl is summarized by the US EPA (2005a) as "suggestive evidence of carcinogenic potential" based on increased incidence of urinary bladder tumours in rats and liver tumours in mice after biphenyl exposure (Li et al. 2016).

In summary, we demonstrated that the concentrations calculated for these targeted aromatic compounds were higher in the B0 gas phase compared to GTL and RME gas phase. Thus, potentially hazardous air pollutants, in particular aromatic compounds, were determined with the highest concentrations in the gas phase and on the PM of B0 combustion aerosol. This implies the potential benefits of a change in fuel type from a health perspective.

Strengths and limitations

This study was carried out under realistic exposure conditions to gain important information on the exposure situation of the mine workers. The choice of this sampling place and the sampling itself has some limitations. The LHD vehicles used are optimized for the use of B0 fuel and, thus, exposure profiles of GTL and RME could be influenced by non-optimal engine settings. As the sampling was conducted without movement of the LHD vehicle the influence of abrasion of break and tire wear cannot be included in this study. An advantage of this setup is that the analysis of elemental composition of the combustion particles is not influenced by elements resulting from abrasion. Moreover, the sampling of $PM_{2.5}$, $PM_{0.25}$, and gas phase enabled a comprehensive characterization of the combustion aerosol of these fuels. The advanced data analysis and evaluation using GC×GC-ToFMS enabled a group-type comparison of methylated PAHs as well as a semi-quantification of targeted unsubstituted PAHs and, thus, the determination of BaP_{TEQ} values. Furthermore, gas phase was sampled at two sampling positions, including the position of the LHD operator, which enabled the assessment of a realistic exposure profile of VOCs for those operators. Based on the chemical characteristics, including the amount of metals and aromatic species released by the combustion of the different fuel types, which reflect compounds of potential health concern, we were able to identify B0 as fuel that released the highest amount of compounds of potential health concern in comparison to GTL and RME.

Conclusion

A decreased release of greenhouse gases, less environmental impact, and a reduced dependency of developing countries on fossil fuels are key factors of sustainable development. In this study, we wanted to evaluate a possible improvement of the exposure situation when exchanging fossil fuel with alternative fuels (GTL, RME). We demonstrated that

chemical compounds such as (methylated) PAHs, metal elements (Cu, Fe), and other aromatic species are released from heavy-duty machinery to a greater extent when fueled with B0 compared to GTL and RME. Moreover, the calculated BaP_{TEQ} value was highest for B0, followed by RME and GTL. Gas phase analysis of the different fuels showed highest concentrations for the targeted aromatic species (BTX, naphthalene, biphenyl) released from B0 followed by GTL and RME. The concentration of these compounds was still elevated at the position of the LHD operator. This implies potential adverse health effects for workers operating this heavy-duty machinery. The use of GTL and RME would release less (methylated) PAHs, metals, and other aromatic species compared to B0, which could consequently lead to a lower toxicological potential of the combustion aerosol. Nevertheless, the use of GTL and RME would still lead to substantial amounts of (methylated) PAHs and VOCs such as benzene and toluene, which should not be neglected.

Future studies should focus on the biological evaluation of these aerosols and their potential toxicological response, as research on the toxicological potential of distinct aerosol components such as methylated PAHs is still limited. Furthermore, we suggest the implementation of TEF values for methylated PAHs to ensure a more comprehensive toxicological evaluation of complex aerosol samples.

Supplementary Information The online version contains supplementary material available at https://doi.org/10.1007/s11869-022-01287-9.

Acknowledgements The authors thank LECO Europe for technical support and for providing the software ChromaTOF Tile for GC×GC data evaluation. Furthermore, we thank Dr. Philip Wenig for the support in data evaluation with the evaluation software OpenChrom (Lablicate). We thank Sasol Limited for the fuel supply and fuel characterization. We also thank ASG Analytik-Service for fuel and lube oil characterization. We further like to thank the management and staff at Impala Platinum Limited for assistance with sampling. The authors would like to thank Dr. Jürgen Schnelle-Kreis and Dr. Hendryk Czech for their fruitful discussions and ideas regarding this paper. Finally, we would like to thank Prof. Dr. Tuulia Hyötyläinen for her support as PhD thesis committee member.

Author contribution All authors, in particular PF, GLG, JO, and NG, contributed to the study conception and design. Material preparation, data collection, and analysis were performed by NG, JO, MW, MJ, GJ, and BM. Interpretation of results was performed by NG, JO, and TG. The concept for the manuscript was elaborated by NG, JO, TG, and RZ. The first draft of the manuscript was written by NG, and all authors commented on previous versions of the manuscript. All authors read and approved the final manuscript.

Funding Open Access funding enabled and organized by Projekt DEAL. We acknowledge the funding provided by the University of Pretoria and the National Research Foundation of South Africa (NRF, grant number 105807) and the support by the German Federal Ministry of Education and Research (BMBF, research contract 01DG17023).

Data availability The datasets used and/or analyzed during the current study are available from the first author on reasonable request. (Please contact nadine.gawlitta@helmholtz-muenchen.de).

Declarations

Ethics approval Not applicable.

Consent to participate Not applicable.

Consent for publication Not applicable.

Competing interests The authors declare no competing interests.

References

Abdel-Shafy HI, Mansour MSM (2016) A review on polycyclic aromatic hydrocarbons: source, environmental impact, effect on human health and remediation. Egypt J Pet 25(1):107–123 https://doi.org/10.1016/j.ejpe.2015.03.011

Andersson JT, Achten C (2015) Time to say goodbye to the 16 EPA PAHs? Toward an up-to-date use of PACs for environmental purposes. Polycyclic Aromat Compd 35(2–4):330–354 https://doi.org/10.1080/10406638.2014.991042

Arzamendi G, Arguiñarena E, Campo I, Zabala S, Gandía LM (2008) Alkaline and alkaline-earth metals compounds as catalysts for the methanolysis of sunflower oil. Catal Today 133–135:305–313 https://doi.org/10.1016/j.cattod.2007.11.029

Bluhm K, Heger S, Seiler T-B, Hallare AV, Schäffer A, Hollert H (2012) Toxicological and ecotoxicological potencies of biofuels used for the transport sector—a literature review. Energy Environ Sci 5(6):7381–7392

Boström CE, Gerde P, Hanberg A, Jernström B, Johansson C, Kyrklund T, Rannug A, Törnqvist M, Victorin K, Westerholm R (2002) Cancer risk assessment, indicators, and guidelines for polycyclic aromatic hydrocarbons in the ambient air. Environ Health Perspect 110 Suppl 3(Suppl 3):451–488 https://doi.org/10.1289/ehp.110-1241197

Chow JC, Watson JG, Chen LWA, Chang MCO, Robinson NF, Trimble D, Kohl S (2007) The IMPROVE_A temperature protocol for thermal/optical carbon analysis: maintaining consistency with a long-term database. J Air Waste Manag Assoc 57(9):1014–1023. https://doi.org/10.3155/1047-3289.57.9.1014

Czech H, Stengel B, Adam T, Sklorz M, Streibel T, Zimmermann R (2017) A chemometric investigation of aromatic emission profiles from a marine engine in comparison with residential wood combustion and road traffic: implications for source apportionment inside and outside sulphur emission control areas. Atmos Environ 167:212–222. https://doi.org/10.1016/j.atmosenv.2017.08.022

Diab J, Streibel T, Cavalli F, Lee SC, Saathoff H, Mamakos A, Chow JC, Chen LWA, Watson JG, Sippula O, Zimmermann R (2015) Hyphenation of a EC/OC thermal–optical carbon analyzer to photo-ionization time-of-flight mass spectrometry: an off-line aerosol mass spectrometric approach for characterization of primary

and secondary particulate matter. Atmos Meas Tech 8(8):3337–3353. https://doi.org/10.5194/amt-8-3337-2015
Gautam S, Patra AK, Sahu SP, Hitch M (2018) Particulate matter pollution in opencast coal mining areas: a threat to human health and environment. Int J Min Reclam Environ 32(2):75–92 https://doi.org/10.1080/17480930.2016.1218110
Hussain M, Madl P, Khan A (2011) Lung deposition predictions of airborne particles and the emergence of contemporary diseases, Part-I. Health 2(2):51–59
Kang HJ, Lee SY, Kwon JH (2016) Physico-chemical properties and toxicity of alkylated polycyclic aromatic hydrocarbons. J Hazard Mater 312:200–207. https://doi.org/10.1016/j.jhazmat.2016.03.051
Kislov VV, Sadovnikov AI, Mebel AM (2013) Formation mechanism of polycyclic aromatic hydrocarbons beyond the second aromatic ring. J Phys Chem A 117(23):4794–4816. https://doi.org/10.1021/jp402481y
Kleeman MJ, Riddle SG, Robert MA, Jakober CA (2008) Lubricating oil and fuel contributions to particulate matter emissions from light-duty gasoline and heavy-duty diesel vehicles. Environ Sci Technol 42(1):235–242. https://doi.org/10.1021/es071054c
Kumar AV, Kothiyal NC, Kumari S, Mehra R, Parkash A, Sinha RR, Tayagi SK, Gaba R (2014) Determination of some carcinogenic PAHs with toxic equivalency factor along roadside soil within a fast developing northern city of India. J Earth Syst Sci 123(3):479–489. https://doi.org/10.1007/s12040-014-0410-7
Kuranchie FA, Angnunavuri PN, Attiogbe F, Nerquaye-Tetteh EN (2019) Occupational exposure of benzene, toluene, ethylbenzene and xylene (BTEX) to pump attendants in Ghana: implications for policy guidance. Cogent Environ Sci 5(1):1603418
Kwon H-S, Ryu MH, Carlsten C (2020) Ultrafine particles: unique physicochemical properties relevant to health and disease. Exp Mol Med 52(3):318–328. https://doi.org/10.1038/s12276-020-0405-1
Lam MM, Bülow R, Engwall M, Giesy JP, Larsson M (2018) Methylated PACs are more potent than their parent compounds: a study of aryl hydrocarbon receptor-mediated activity, degradability, and mixture interactions in the H4IIE-luc assay. Environ Toxicol Chem 37(5):1409–1419. https://doi.org/10.1002/etc.4087
Li X, Huang Z, Wang J, Zhang W (2007) Particle size distribution from a GTL engine. Sci Total Environ 382(2–3):295–303. https://doi.org/10.1016/j.scitotenv.2007.04.032
Li Z, Hogan KA, Cai C, Rieth S (2016) Human health effects of biphenyl: key findings and scientific issues. Environ Health Perspect 124(6):703–712. https://doi.org/10.1289/ehp.1509730
Lin YC, Tsai CJ, Wu YC, Zhang R, Chi KH, Huang YT, Lin SH, Hsu SC (2015) Characteristics of trace metals in traffic-derived particles in Hsuehshan Tunnel, Taiwan: size distribution, potential source, and fingerprinting metal ratio. Atmos Chem Phys 15(8):4117–4130. https://doi.org/10.5194/acp-15-4117-2015
Lipsky EM, Robinson AL (2006) Effects of dilution on fine particle mass and partitioning of semivolatile organics in diesel exhaust and wood smoke. Environ Sci Technol 40(1):155–162. https://doi.org/10.1021/es050319p
Llamas A, Al-Lal A-M, García-Martínez M-J, Ortega MF, Llamas JF, Lapuerta M, Canoira L (2017) Polycyclic aromatic hydrocarbons (PAHs) produced in the combustion of fatty acid alkyl esters from different feedstocks: Quantification, statistical analysis and mechanisms of formation. Sci Total Environ 586:446–456 https://doi.org/10.1016/j.scitotenv.2017.01.180
Lu T, Huang Z, Cheung CS, Ma J (2012) Size distribution of EC, OC and particle-phase PAHs emissions from a diesel engine fueled with three fuels. Sci Total Environ 438:33–41. https://doi.org/10.1016/j.scitotenv.2012.08.026
Mason YC, Schoonraad G-L, Orasche J, Bisig C, Jakobi G, Zimmermann R, Forbes PBC (2020) Comparative sampling of gas phase volatile and semi-volatile organic fuel emissions from a combustion aerosol standard system. Environ Technol Innov 19:100945 https://doi.org/10.1016/j.eti.2020.100945
Mihajlović V, Grba N, Suđi J, Eichert D, Krajinović S, Gavrilov MB, Marković SB (2021) Assessment of occupational exposure to BTEX in a petrochemical plant via urinary biomarkers. Sustainability 13(13):7178
Mohadesi M, Hojabri Z, Moradi G (2014) Biodiesel production using alkali earth metal oxides catalysts synthesized by sol-gel method. Biofuel Res J 1(1):30–33
Møller P, Scholten RH, Roursgaard M, Krais AM (2020) Inflammation, oxidative stress and genotoxicity responses to biodiesel emissions in cultured mammalian cells and animals. Crit Rev Toxicol 50(5):383–401 https://doi.org/10.1080/10408444.2020.1762541
Moon G, Lee Y, Choi K, Jeong D (2010) Emission characteristics of diesel, gas to liquid, and biodiesel-blended fuels in a diesel engine for passenger cars. Fuel 89:3840–3846. https://doi.org/10.1016/j.fuel.2010.07.009
Nisbet IC, Lagoy PK (1992) Toxic equivalency factors (TEFs) for polycyclic aromatic hydrocarbons (PAHs). Regul Toxicol Pharmacol 16(3):290–300
Richter-Brockmann S, Achten C (2018) Analysis and toxicity of 59 PAH in petrogenic and pyrogenic environmental samples including dibenzopyrenes, 7H-benzo[c]fluorene, 5-methylchrysene and 1-methylpyrene. Chemosphere 200:495–503 https://doi.org/10.1016/j.chemosphere.2018.02.146
Ryu K (2010) The characteristics of performance and exhaust emissions of a diesel engine using a biodiesel with antioxidants. Bioresour Technol 101(Suppl 1):S78-82. https://doi.org/10.1016/j.biortech.2009.05.034
Sakthivel R, Ramesh K, Purnachandran R, Shameer PM (2018) A review on the properties, performance and emission aspects of the third generation biodiesels. Renew Sustain Energy Rev 82:2970–2992
Salo L, Rönkkö T, Saarikoski S, Teinilä K, Kuula J, Alanen J, Arffman A, Timonen H, Keskinen J (2021) Concentrations and size distributions of particle lung-deposited surface area (LDSA) in an underground mine. Aerosol Air Qual Res 21:200660. https://doi.org/10.4209/aaqr.200660
Selby TW, Bosch RJ, Fee DC (2005) Phosphorus additive chemistry and its effects on the phosphorus volatility of engine oils. J ASTM Int 2(9) https://doi.org/10.1520/JAI12977
Shrivastava MK, Lipsky EM, Stanier CO, Robinson AL (2006) Modeling semivolatile organic aerosol mass emissions from combustion systems. Environ Sci Technol 40(8):2671–2677. https://doi.org/10.1021/es0522231
Sun Y, Miller III CA, Wiese TE, Blake DA (2014) Methylated phenanthrenes are more potent than phenanthrene in a bioassay of human aryl hydrocarbon receptor (AhR) signaling. Environ Toxicol Chem 33(10):2363–2367 https://doi.org/10.1002/etc.2687
Tavizón-Pozos JA, Chavez-Esquivel G, Suárez-Toriello VA, Santolalla-Vargas CE, Luévano-Rivas OA, Valdés-Martínez OU, Talavera-López A, Rodriguez JA (2021) State of art of alkaline earth metal oxides catalysts used in the transesterification of oils for biodiesel production. Energies 14(4):1031
Traviss N, Thelen BA, Ingalls JK, Treadwell MD (2010) Biodiesel versus diesel: a pilot study comparing exhaust exposures for employees at a rural municipal facility. J Air Waste Manag Assoc (1995) 60(9):1026–1033 https://doi.org/10.3155/1047-3289.60.9.1026
Unosson J, Kabéle M, Boman C, Nyström R, Sadiktsis I, Westerholm R, Mudway IS, Purdie E, Raftis J, Miller MR, Mills NL, Newby DE, Blomberg A, Sandström T, Bosson JA (2021) Acute cardiovascular effects of controlled exposure to dilute

petrodiesel and biodiesel exhaust in healthy volunteers: a crossover study. Part Fibre Toxicol 18(1):22. https://doi.org/10.1186/s12989-021-00412-3

van Steen E, Claeys M (2008) Fischer-Tropsch catalysts for the biomass-to-liquid (BTL)-process. Chemi Eng Technol Ind Chem-Plant Equip-Process Eng-Biotechnol 31(5):655–666

Wattrus MC, Biffi M, Pretorius CJ, Jacobs D (2016) Assessing stationary laboratory test methods for underground mining vehicles to determine their suitability in replicating real-world emissions. Mine Ventilation Society of South Africa 2016 Conference: The increasing relevance of the mine ventilation profession in a highly regulated and cost constrained environment, 1–2 September 2016, Emperors Palace, Johannesburg, p 37–44

World Health Organization (2021) WHO global air quality guidelines: particulate matter (PM2.5 and PM10), ozone, nitrogen dioxide, sulfur dioxide and carbon monoxide. Geneva, World Health Organization

Yasin MHM, Ali MA, Mamat R, Yusop AF, Ali MH (2019) Chapter 11 - Physical properties and chemical composition of biofuels. In: Basile A, Dalena F (eds) Second and Third Generation of Feedstocks. Elsevier, pp 291–320

Yost EE, Galizia A, Kapraun DF, Persad AS, Vulimiri SV, Angrish M, Lee JS, Druwe IL (2021) Health effects of naphthalene exposure: a systematic evidence map and analysis of potential considerations for dose–response evaluation. Environ Health Perspect 129(7):076002. https://doi.org/10.1289/EHP7381

Zaharin MSM, Abdullah NR, Najafi G, Sharudin H, Yusaf T (2017) Effects of physicochemical properties of biodiesel fuel blends with alcohol on diesel engine performance and exhaust emissions: a review. Renew Sustain Energy Rev 79:475–493 https://doi.org/10.1016/j.rser.2017.05.035